Available online at www.sciencedirect.com
SCIENCE DIRECT®
International Journal of Heat and Mass Transfer 47 (2004) 5591–5601
International Journal of HEAT and MASS TRANSFER
www.elsevier.com/locate/ijhmt

Bubble dynamics in microchannels. Part II: two parallel microchannels

H.Y. Li, F.G. Tseng, Chin Pan *

Department of Engineering and System Science, National Tsing Hua University, Hsinchu 30043, Taiwan, ROC

Received 9 December 2003; received in revised form 7 February 2004
Available online 18 September 2004

Abstract

The present work investigates experimentally the bubble dynamics in two parallel trapezoidal microchannels with a hydraulic diameter of 47.7 μm for both channels. The fabrication process of the two parallel microchannels employs a silicon bulk micromachining and anodic bounding process. The results of this study demonstrate that the bubble growth and departure is generally similar to that in a single microchannel, i.e., bubbles, in general, grow linearly with time and their departure is governed by surface tension and drag due to bulk two-phase flow. For the two low mass flow rates, the growth of bubble in slug flow is also investigated. It is found that the bubble grows in the axial direction both forward and backward with its length increases exponentially due to evaporation of the thin liquid film between the bubble and heating wall. However, the coefficient of exponent is much smaller than that caused by evaporation due to the limitation effect of liquid pressure around the bubble.

Keywords: Microchannels; Bubble dynamics; Onset nucleate boiling; Boiling heat transfer; Slug flow

1. Introduction

A compact evaporator usually contains many parallel microchannels. Boiling heat transfer and associated two-phase flow in a parallel microchannel system may be different from that in a single microchannel. The channel-to-channel interactions among channels may affect bubble nucleation, bubble interactions as well as associated two-phase flow. Indeed, two-phase flow instability has been reported in several previous studies of boiling heat transfer in minichannels. For example, Kandlikar et al. [1] reported flow instability in electrically heated multi-minichannel evaporators consisting of six parallel minichannels with visual confirmation of complete flow reversal in some of the channels. Li et al. [2] reported two-phase flow instability of boiling in a two parallel triangular microchannels at high heating power under relatively low flow conditions. Large amplitude oscillations in inlet and outlet temperatures and pressure drop through the channel were reported.

In ordinary sized parallel boiling channels, channel-to-channel interactions are through the boundary conditions that the summation of flow rate through each channel is equal to the total mass flow rate and the pressure drop across each channel is the same due to their common inlet and outlet reservoirs [3]. For parallel microchannels channel-to-channel interactions could be more complicated than for ordinary sized channels. This is because the dividing wall between two

* Corresponding author. Tel.: +886 3 5725363; fax: +886 3 5720724.
E-mail address: cpan@ess.nthu.edu.tw (C. Pan).

0017-9310/$ - see front matter © 2004 Elsevier Ltd. All rights reserved.
doi:10.1016/j.ijheatmasstransfer.2004.02.032

Nomenclature

A_c	cross-section area of channel (m^2)	R_0	initial bubble radius (μm)
G	mass flux (kg/m^2s)	T_w	wall temperature (°C)
i_{lv}	the latent heat of evaporation (J/kg)	T_{surf}	heater surface temperature (°C)
L	channel length (mm)	T_w	wall temperature (°C)
L_0	initial bubble length of the bubble in slug flow (μm)	T_{sat}	saturation temperature (°C)
$L(t)$	time evolution of bubble length in slug flow (μm)	t	time (ms)
		Greek symbols	
L_r	bubble length ratio, $L(t)/L_0$	ρ_v	the density of vapor (kg/m^3)
P_H	heated perimeter of channel (μm)	ΔP	pressure drop through the channel (Pa)
q''	heat flux (kW/m^2)	β	coefficient of exponent for bubble growth in slug flow (1/s)
$\dot{R}$	bubble growth rate (μm/s)	σ	surface tension (N/m)
R_D	bubble departure radius (μm)		

neighboring channels must be very thin and the two channels could interact with each other through the conduction of the wall [4]. For example, bubble nucleation and subsequent boiling process will remove much heat from the wall and possibly suppress boiling nucleation or reduce the bubble growth rate in the neighboring channel. The influence could also be hydrodynamic. In the microchannel, the pressure drop is very sensitive to the void fraction. The bubble nucleation and subsequent bubble growth would increase the pressure drop in that particular channel. As a result, the flow rate through that channel could be significantly reduced and the flow rate through other channels could be significantly increased and, therefore, the bubble dynamics in another channel and vice versa.

It is, therefore, of significant interest to explore the bubble dynamics in multi-parallel microchannels. In the literature, research works on bubble dynamics in parallel microchannels are rare. Hetsroni et al. [5] reported boiling incipience and growth of individual bubble in parallel microchannels of isosceles triangle with a base of 200–310 μm. Steinke and Kandlikar [6] reported rapid bubble growth in 200 μm^2 microchannel causing reversed flow in a parallel microchannel. The objective of the present study is to investigate bubble dynamics in two parallel trapezoid microchannels. The observation and analysis will be compared with that found in a single microchannel [7].

2. Experimental

The experimental setup, consisting of a test section, a syringe pump, a heating module and a flow visualization system, is basically the same as that in Lee et al. [7] except for the test section. The test section for this study is

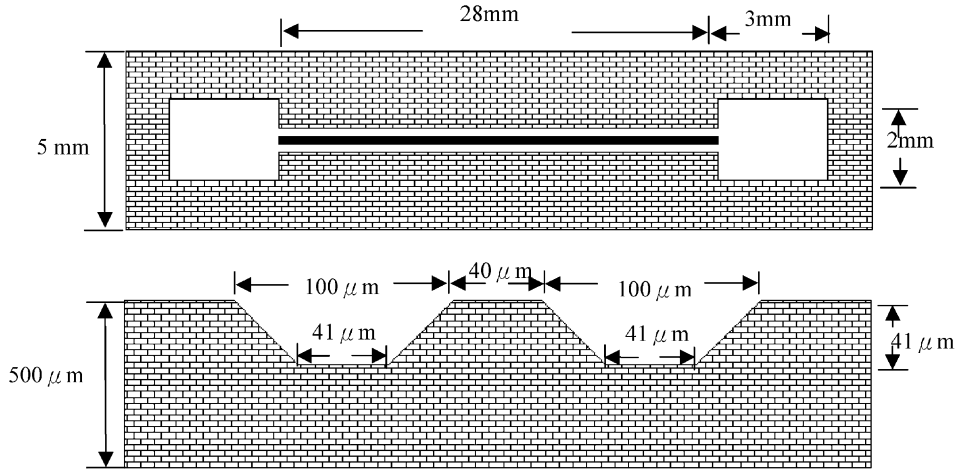

Fig. 1. The top and cross-section views of the test section with a two parallel trapezoid microchannels (length shown not in scale).

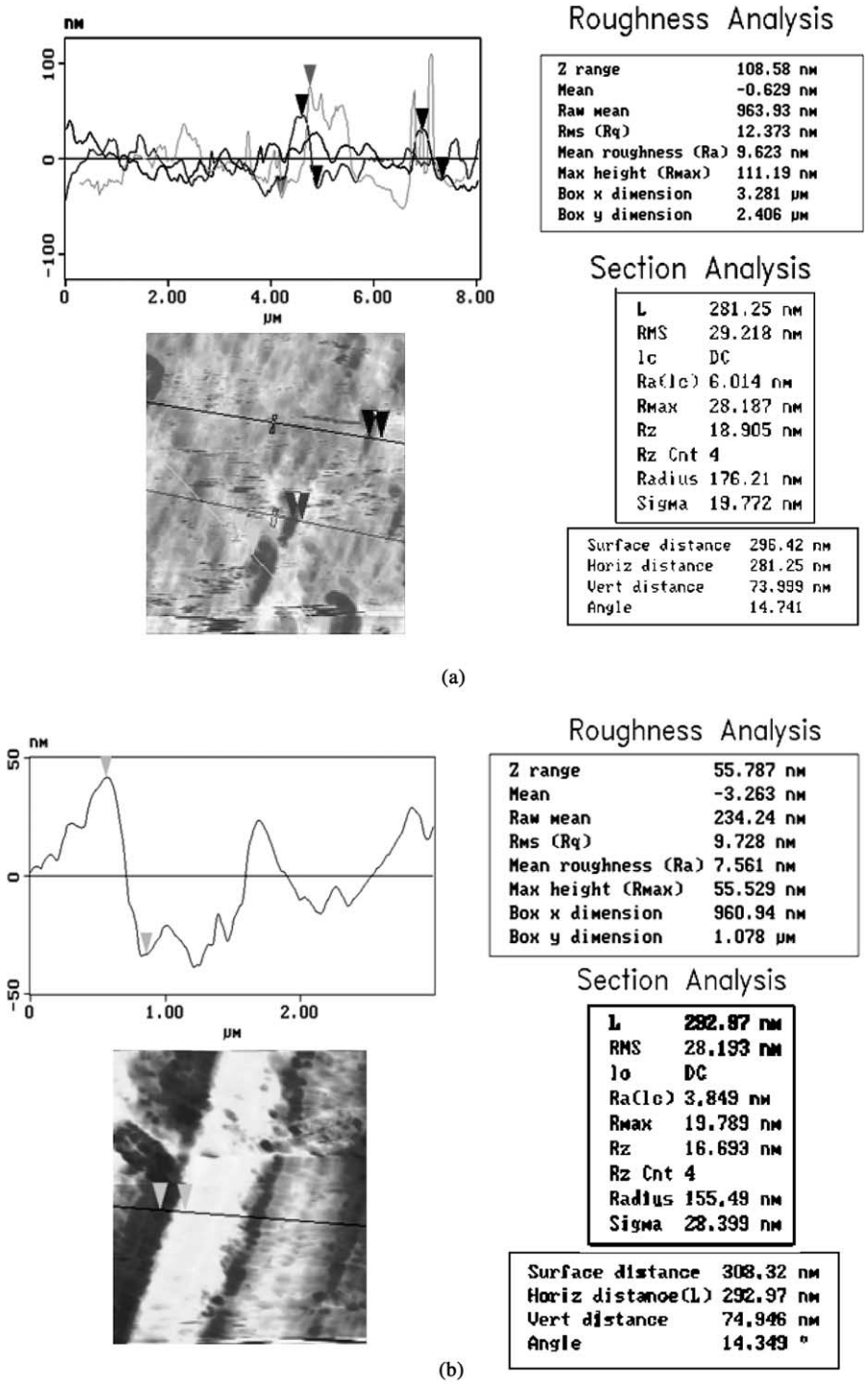

Fig. 2. Surface roughness based on section analysis and line profiles using an atomic force microscope: (a) bottom wall and (b) side wall.

a 5-mm wide silicon stripe, which is made of P-type ⟨100⟩ orientation wafer and is etched with two parallel trapezoid microchannels on its top surface. Fig. 1 illustrates the top and cross-sectional views of the test section. For both channels, the top and bottom widths are 100 and 41 μm, respectively, and the depth is 41 μm

resulting a hydraulic diameter for both channels of 47.7 μm. The top width for the central island between two channels is 40 μm. The channel length is 28 mm resulting a length–diameter ratio of 587. Only the central 20 mm is heated. The dimensions for both inlet and outlet sumps are 3 mm × 2 mm.

The fabrication process of the two parallel microchannels employs a silicon bulk micromachining and anodic bounding process [2]. The surface roughness of the channels is examined by an atomic force microscope including section analysis and line profiles of both bottom and side walls (see Fig. 2). The root mean square roughness for a small area of $8 \times 8\,\mu m^2$ and $3 \times 3\,\mu m^2$ is 15.8 nm and 17.9 nm for bottom and side walls, respectively. These values may not be universal for the whole channel surface. The maximum heights are 237 nm and 264 nm for the bottom and side surfaces, respectively. The maximum height is considered to be more representative for a wet-etched channel. However, for the side wall scratches in the axial direction are found, possibly due to that a simple mask was used before wet etching.

Similar to the single-channel experiments [7], the temperature at the inlet and outlet reservoirs are measured using T-type thermocouples and the inlet pressure is

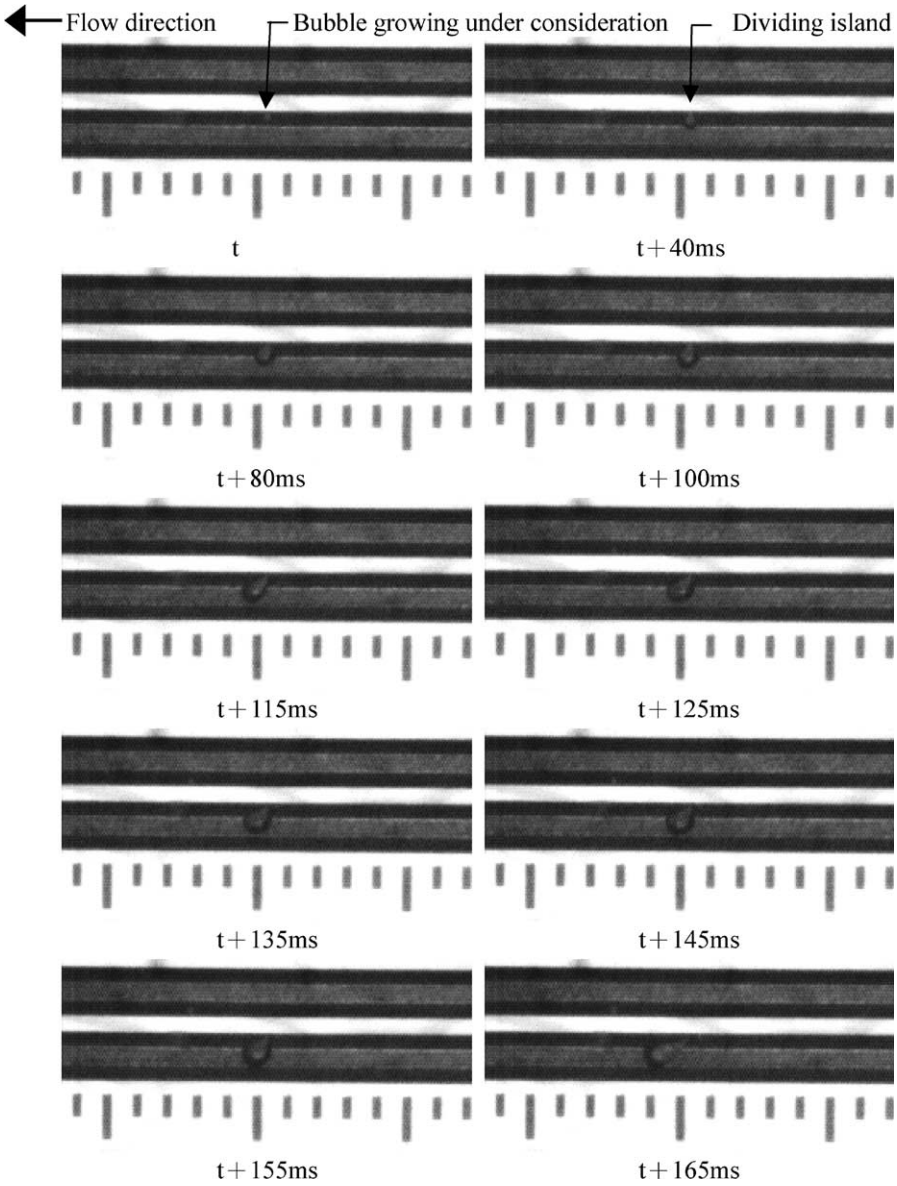

Fig. 3. Sequential images of bubble growing ($G = 269\,kg/m^2s$, $q'' = 303\,kW/m^2$).

measured by a pressure transducer. The variation of inlet pressure reflects the change of pressure drop through the channel as the outlet container is exposed to the atmosphere. The channel wall heat flux and various heat losses are evaluated based on the similar approach as for the single-channel study [7].

2.1. Uncertainty analysis

The uncertainties in temperature measurements are ±0.6 °C and ±1 °C for K- and T-type thermocouples. The uncertainty in flow rate measurements is ±4.8%. The uncertainty in surface heat flux is estimated to be from ±4.47% to ±58.8% with an average uncertainty of ±14.9%. The highest uncertainty appears for the case of $G = 269\,\mathrm{kg/m^2 s}$ and $q'' = 12.4\,\mathrm{kW/m^2}$. For a given mass flow rate, the heat flux uncertainty generally decreases with increasing heat flux.

2.2. Experimental procedure

The experimental procedure employed in this study is also similar to that for the single-channel work [7]. The working fluid, i.e., the de-ionized water, is first boiled in a beaker to remove the dissolved gases in the water. Subsequently, the de-ionized water is poured into the injecting tube of the syringe pump after it is cooled down to room temperature. Subsequently, the working fluid is pushed into the channels at a specific flow rate. The heating power is switched on to a specific level once

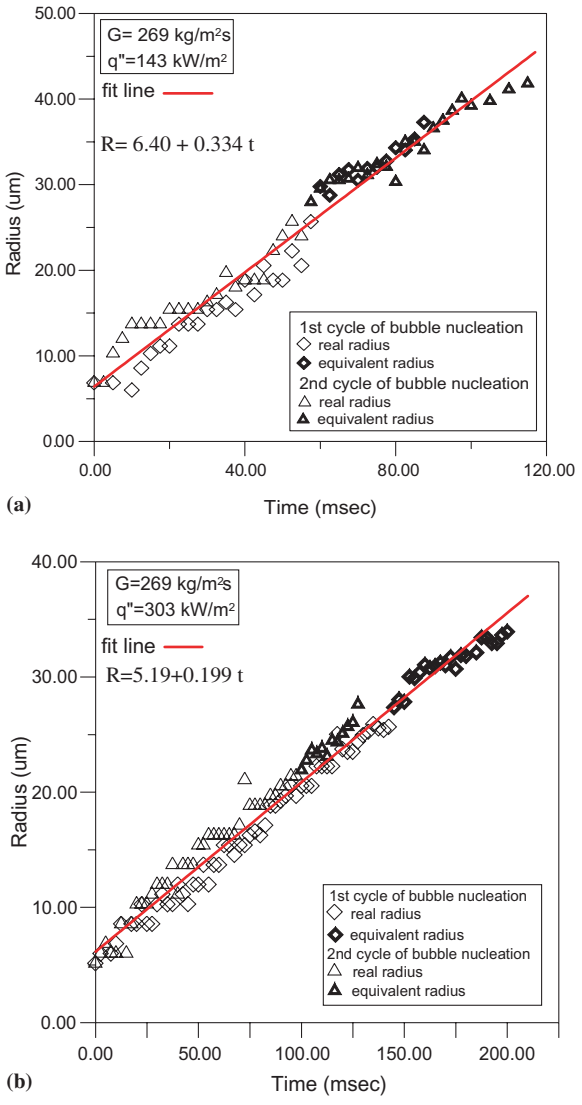

Fig. 4. Typical time evolution of bubble radius for $G = 269\,\mathrm{kg/m^2 s}$: (a) $q'' = 143\,\mathrm{kW/m^2}$ and (b) $q'' = 303\,\mathrm{kW/m^2}$.

the inlet pressure reaches the steady state. This usually takes about 1.5–2.0 h. For this study the heating power and thus the heating surface temperatures is varied to investigate its effects on bubble dynamics in two parallel microchannels at a given flow rate.

3. Results and discussion

3.1. Onset of nucleate boiling

The bubble dynamics presented in this work is for those bubbles at the location of onset of nucleate boiling (ONB) under a given condition. The general trend of heat flux on ONB location is similar to that in a single microchannel [7] as well as in a ordinary sized channel, i.e., at a given flow rate, the ONB location generally moves toward upstream as the heat flux is increased.

3.2. Bubble growth

Fig. 3 illustrates a sequence of bubble growing at a low mass flux of 269 kg/m^{2}s and heat flux of 303 kW/m^2. A single bubble is nucleated from the central wall and grows from its nucleation site. For $t \leqq 100$ ms, the bubble grows spherically. For $t > 100$ ms, the bubble is distorted due to drag of the bulk flow. At $t + 165$ ms, the bubble touches the other side and is actually departing. The bubble diameter at the moment of departure is defined as the departure diameter.

Fig. 4(a) and (b) illustrates the typical time evolution of bubble radius for two cycles of $G = 269$ kg/m^{2}s and two different heat fluxes. The bubble grows linearly, similar to the typical growth pattern in a single microchannel [7], suggesting the bubble growth is inertia controlled. The bubble growth rates for both the cases are 0.334 and 0.199 μm/ms, respectively. For the case of $q'' = 190$ kW/m^2 the bubble grows following approximately the square root of time (see Fig. 5) indicating that the bubble growth may be diffusion controlled. This is

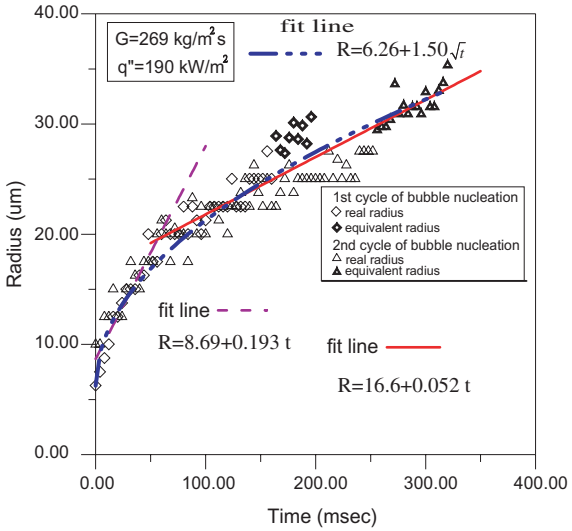

Fig. 5. An unusual bubble growth pattern, $G = 269$ kg/m^{2}s, $q'' = 190$ kW/m^2.

Table 1
Bubble growth rate ($\dot{R}$) and initial bubble radius (R_0) under various conditions

q'' (kW/m^2)	T_w (°C)	T_{sat}[a] (°C)	$\dot{R}$ (μm/ms)	R_0 (μm)	Remarks
G = 105 (kg/m^{2}s)					
17.8	106	102	4.29 ± 0.88	~7[b]	Bubble waiting period; reversed flow present
53.9	112	105	1.62 ± 0.11	~7[b]	Bubble waiting period and reversed flow present
121	124	108	2.27 ± 0.39	8.70 ± 1.59	Bubble waiting period occurs intermittently, Reversed flow present
G = 269 (kg/m^{2}s)					
12.3	97	104	0.087 ± 0.001	4.32 ± 0.29	$T_w < T_{sat}$; reversed flow present
30.1	103	104	0.175 ± 0.003	7.27 ± 0.32	$T_w < T_{sat}$; reversed flow present
65.4	108	106	1.32 ± 0.080	8.15 ± 1.16	Reversed flow present
143	118	110	0.334 ± 0.008	6.40 ± 0.44	Reversed flow present
190	132	111	0.193 ± 0.014[c]	8.69 ± 0.41	Reversed flow present
245	146	114	0.211 ± 0.02[c]	8.64 ± 0.51	Reversed flow present
303	157	115	0.147 ± 0.002	6.16 ± 0.20	Reversed flow present
G = 555 (kg/m^{2}s)					
70.6	94	104	0.306 ± 0.008	6.82 ± 0.29	$T_w < T_{sat}$
123	112	103	4.12 ± 0.23	8.48 ± 0.28	
233	131	105	15.0 ± 8.5	9.32 ± 0.3	

[a] Corresponding to system pressure = (P_{in} + 1 atm)/2.
[b] Estimated from bubble size of waiting period.
[c] Initial bubble growth rate.

an unusual growth pattern in the two parallel microchannels of this study and in the single microchannel [7].

Because the flow rate is relatively high for these cases, the bubbles are distorted for various different cases due to constrain of the top and bottom walls in the vertical direction and flow drag after their radius reaches a critical size of about 30 μm as indicated in Figs. 4 and 5. This critical size for transition from isotropic to anisotropic growth is closed to that observed in a single microchannel [7]. After this critical value, the bubble radius is defined as an equivalent radius of the bubble with the same projected area.

Table 1 summarizes the bubble growth rate and initial bubble radius under various different combinations of mass flux and heat flux. The bubble growth rates range from 0.087 to 15.0 μm/m s. Such a growth rate is with the same order of magnitude as most of bubble growth rates in a single microchannel, but is much smaller than that given by the Rayleigh equation [7]. As discussed in Lee et al. [7], the bubble growth in microchannel is constrained, at least, in the transversal directions. Moreover, the temperature gradient in the transversal directions is expected to be high. Therefore, the bubble growth rate is much smaller than that given by the Rayleigh equation based on the wall superheat. The bubble growth rate increases with increase in heat flux for $G = 555\,\mathrm{kg/m^2 s}$. This is consistent with what would be expected as the increase in heat flux would enhance the evaporation rate and thus the growth rate. However, the situation seems to be reversed for both the cases of low flow rates. Except for the two cases of $T_w < T_{sat}$, the bubble growth rate at low flow rates generally decreases with increase in heat flux. This is somewhat unexpected. However, such a trend is consistent with the variation of ONB locations. As discussed in Ref. [7], the ONB location moves toward upstream and the local water temperature will be close to that at the inlet reservoir as the heat flux is increased. Moreover, following the increase in heating power, the local pressure and so the corresponding saturation temperature is also significantly increased. The increase of pressure and saturation temperature may suppress the bubble growth. Moreover, the two-phase flow in the two parallel microchannels under both low flow rate conditions is unstable, possible caused by channel-to-channel interactions. The effective heat flux and flow rate may not be that of the average value and makes the bubble growth rate more intractable.

Bubble nucleation and growth are also observed for three cases with the wall temperature lower than the saturation temperature corresponding to the system pressure, i.e., the average of inlet and outlet pressure. $G = 269\,\mathrm{kg/m^2 s}$, $q'' = 12.3$ and $30.1\,\mathrm{kW/m^2}$, $G = 555\,\mathrm{kg/m^2 s}$ and $q'' = 70.6\,\mathrm{kW/m^2}$. The bubble nucleation and growth for these three cases are attributed to the dissolved gases in water. For these three cases, the bubble grows with a constant rate of 0.087, 0.175, and 0.306 μm/m s, respectively. Although care had been exercised to minimize dissolved gases in water, it seems to be inevitable using the syringe pump with a plastic injection tube. The water after boiling off gases must be cooled down to pour into the injection tube and some gases may then dissolve in water.

Table 1 also illustrates the initial bubble radius, which is the size of the bubble before its growing, i.e., at $t = 0$. The table shows that the initial bubble radius are from 4.3 to 9.3 μm and is quite insensitive to the change of heat flux and mass flux. This may reflect the size of cavity that a bubble is standing.

Fig. 6 shows a comparison of bubble growth rate among the data from two parallel microchannels and single microchannel under various different conditions of heat flux and mass flux. Those six data with $T_w < T_{sat}$ as discussed previously, are due to dissolved gases in the water. The heat flux and mass flux seems to have insignificant effect on bubble growth rate with $T_w < T_{sat}$ of both single microchannel and two parallel microchannels and there is good agreement in bubble growth rate, with a typical value of around 0.2 μm/m s, between single microchannel and two parallel microchannels. Under boiling conditions with $T_w > T_{sat}$, a direct comparison is not possible as the flow rate is not the same. Moreover, reversed flows are present for the system with two parallel microchannels for both $G = 105$ and $269\,\mathrm{kg/m^2 s}$ (see Table 1). Reversed flow also appeared in the single microchannel at the highest heat flux level for each mass flux shown in the figure. Fig. 6 shows that

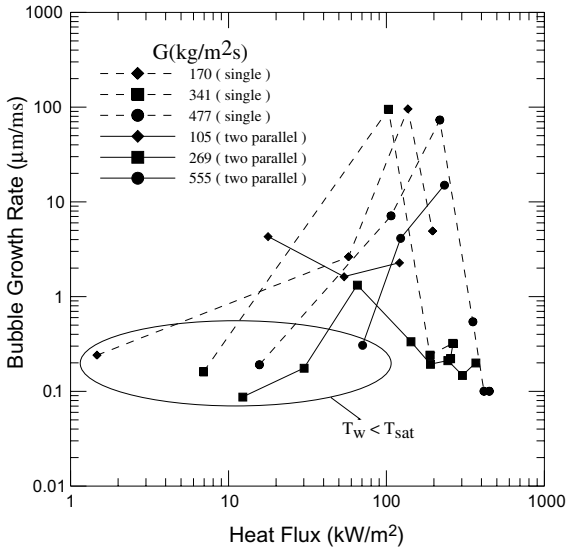

Fig. 6. Comparison of bubble growth rate with single and two parallel microchannels under various different heat flux and mass flux.

for the single microchannel system, the bubble growth rate increases with increase in heat flux at the low heat flux region and decrease with increase in heat flux after it reaches a maximum, as discussed in Ref. [7]. For the system with two parallel microchannels, bubble growth rate increases with increase in heat flux for $G = 477\,\mathrm{kg/m^2 s}$, while a reversed effect is illustrated for $G = 170$ and $341\,\mathrm{kg/m^2 s}$ due to movement of the location of ONB toward upstream and two-phase flow instability as discussed previously.

3.3. Bubble departure diameter

Similar to that in a single microchannel, the bubble departure in two parallel microchannels is also found to be governed by surface tension and drag due to the bulk two-phase flow. As discussed in Ref. [7], following an approach similar to the Levy's model, the bubble departure radius may be correlated as

$$R_D = C_1 \left(\frac{\sigma L}{\Delta P} \right)^{1/2} + C_2 \tag{1}$$

where R_D is the bubble departure radius (μm). Unlike those in a single microchannel [7] the empirical constants C_1 and C_2 are found to be a function of mass flux. For $G = 269\,\mathrm{kg/m^2 s}$, $C_1 = 3.7 \times 10^4$, $C_2 = 31.2$; for $G = 555\,\mathrm{kg/m^2 s}$, there are only three data points, and $C_1 = 4.7 \times 10^4$, $C_2 = 11.7$; for the $G = 105\,\mathrm{kg/m^2 s}$, there is only one datum available. If both set of data from single microchannel and two parallel microchannels are correlated together, 85% of the data can be predicted by Eq. (1) with $C_1 = 7.63 \times 10^4$ and $C_2 = 22.6$ within ±30%.

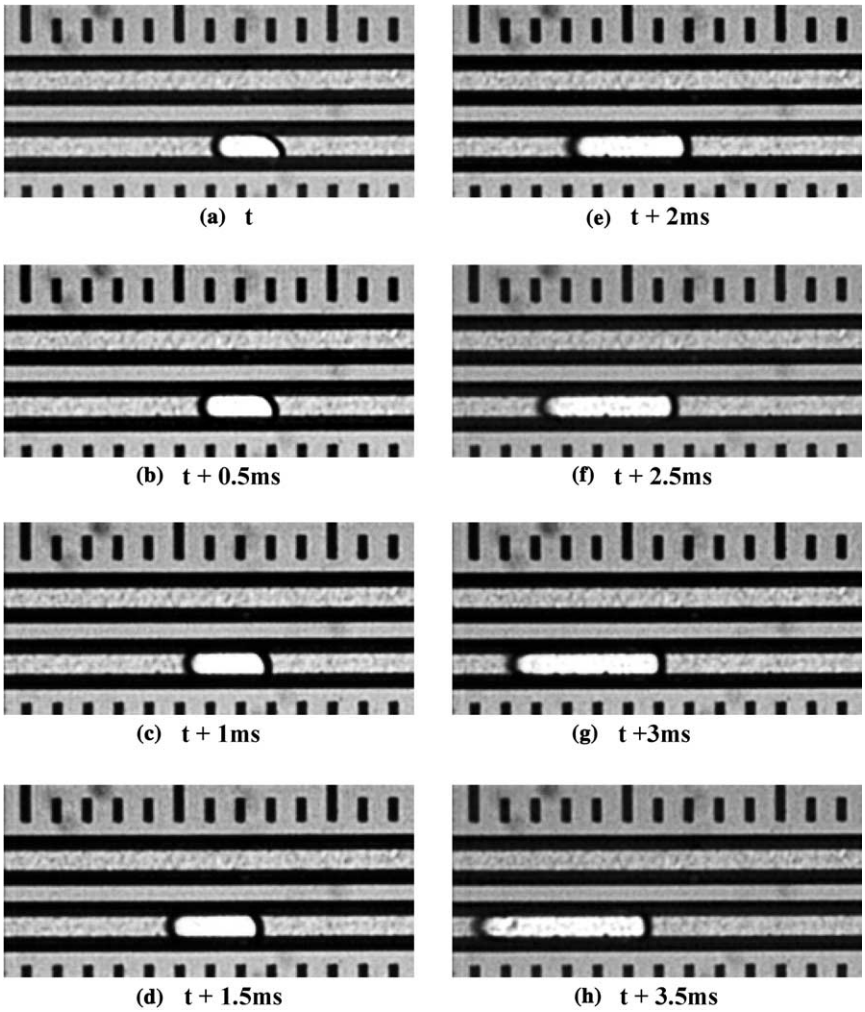

Fig. 7. The exponential growth of bubble in the axial direction, $G = 105\,\mathrm{kg/m^2 s}$, $q'' = 53.9\,\mathrm{kW/m^2}$.

3.4. Growth of bubble in slug flow

For the two low mass flow rates of this study, the growth of bubble in slug flow is also studied. It is found that the bubble expands rapidly in both the forward and backward directions. Such a growth mode may also be present in a single microchannel but was not explored in the companionate paper [7]. Fig. 7 illustrates the bubble growing of this kind for $G = 105\,\mathrm{kg/m^2 s}$ and $q'' = 53.9\,\mathrm{kW/m^2}$. For this case, the center of the bubble has been moved slightly in the flow direction while the bubble is growing. Moreover, Fig. 7(e)–(h) illustrates that the radius of curvature in the bubble front is smaller than that at the bubble tail. Physically, the pressure in the liquid slug near the front end is smaller than the rear end due to the pressure drop through the channel therefore the radius of curvature there is smaller. This should not be attributed to the hysteresis of dynamic contact angle. A thin liquid film is really present between the bubble and tube wall as the dark band, which is primarily due to the sidewall of the trapezoid channel, between the bubble and channel wall is the same as those in the liquid slug between bubbles. If the liquid film dries out, the band will become gray. Significantly, there is no bubble present in the other channel during the course of bubble expansion. This may be explained by the evaporation of the thin liquid film consuming most of the heat from the channel wall and, therefore, suppress the nucleation and/or bubble growth in the other channel.

Fig. 8 demonstrates that the bubble length for the above case grows exponentially with a coefficient of exponent of $0.285 \pm 0.010\,\mathrm{ms^{-1}}$. In the figure, L_r stands for the relative bubble length with respect to the initial bubble length. Such an exponential growth mode is fairly repeatable as shown for five bubbles in sequence. Such an exponential growth mode is also applicable for various cases under the condition of $G = 269\,\mathrm{kg/m^2 s}$ and two of them are shown in Fig. 9(a) and (b).

The growth of bubble in slug flow is mainly governed by the evaporation of thin liquid film around the bubble. On the other hand the pressure field around the bubble may limit the growth of bubble. The test section itself is a small volume for the two-phase mixture. The increase of bubble volume may effectively increase the pressure around the bubble and, therefore, limit the growth of bubble. Indeed, bubble growing and shrinking alternatively has been observed in some of the experiments. Considering both the evaporation and pressure limitation effects, the time rate of bubble length may be modeled as:

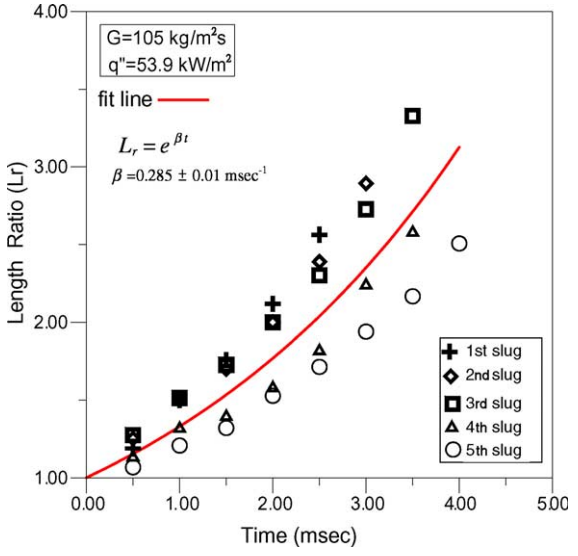

Fig. 8. Time evolution of bubble length ratio for $G = 105\,\mathrm{kg/m^2 s}$, $q'' = 53.9\,\mathrm{kW/m^2}$.

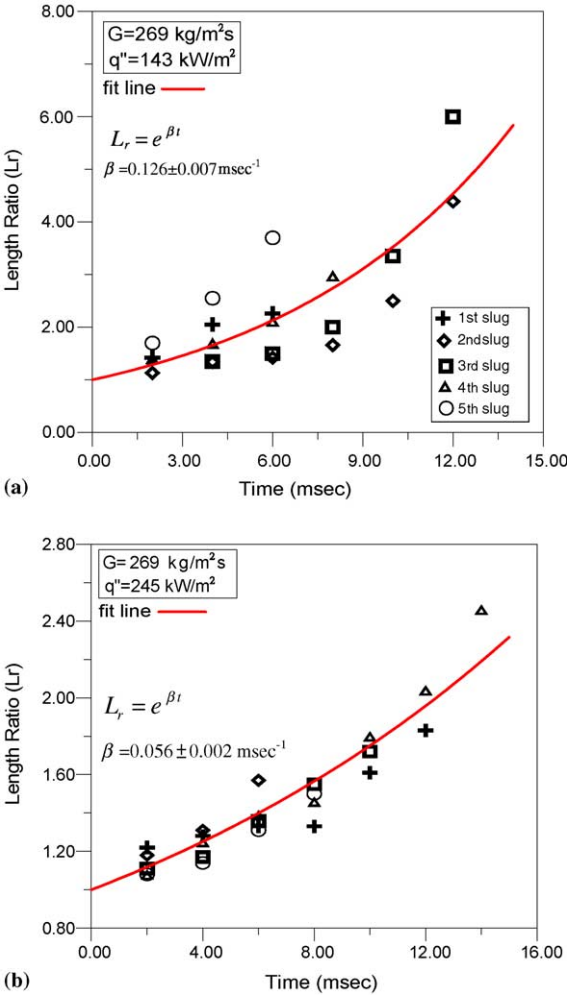

Fig. 9. Time evolution of bubble length ratio for $G = 269\,\mathrm{kg/m^2 s}$: (a) $q'' = 143\,\mathrm{kW/m^2}$ and (b) $q'' = 245\,\mathrm{kW/m^2}$.

$$A_c \frac{dL}{dt} = \frac{qP_H}{i_{lv}\rho_v} L - CA_c L \quad (2)$$

where L is the bubble length at time t, A_c is the cross-sectional area of the bubble; P_H is the heated perimeter; i_{lv} and ρ_v are the latent heat of evaporation and vapor density, respectively; q is the wall heat flux; C is a constant to be determined. Under saturated boiling conditions, it may be assumed that all the heat flux from the channel wall goes to phase change. The first term on the right hand side of Eq. (1) accounts for the increase rate of vapor volume due to evaporation, while the second one accounts for the limitation effect of pressure rise due to an increase in bubble volume.

The integration of Eq. (1) gives

$$\frac{L(t)}{L_0} = \exp(\beta t) \quad (3)$$

where

$$\beta = \frac{q'' P_H}{i_{lv}\rho_v A_c} - C \quad (4)$$

Eq. (3) indicates that the bubble length will grow exponentially if the evaporation effect is dominant over the pressure effect. Indeed, this is the case. The bubble grows exponentially as shown previously in Figs. 7 and 8. With β obtained from the fitting of experimental data, the constant C in Eq. (4) may be evaluated. Table 2 lists the values of $(q'' P_H)/(\rho_v i_{lv} A_c)$, β and C as a function of mass flux and heat flux. There is good agreement between $(q'' P_H)/(\rho_v i_{lv} A_c)$ and β for the case of $G = 105\,\mathrm{kg/m^2 s}$ and $q'' = 17.8\,\mathrm{kW/m^2}$. However, in general, β is much smaller than that due to thin film evaporation, i.e., $(q'' P_H)/(\rho_v i_{lv} A_c)$, and the numerical value for C is generally very large. This indicates the significant effect of pressure limitation on the expansion of bubble in slug flow. It seems to have no general trend for β and C with variation in heat flux and/or mass flux.

Table 2
Coefficient of exponent for bubble growth for various cases

G (kg/m^{2}s)	q'' (kW/m^2)	$(q'' P_H)/(\rho_v i_{lv} A_c)$ (1/s)	β (1/s)	C (1/s)
105	17.8	453	469	−16
105	53.9	1146	285	861
269	12.4	430	23	407
269	30.1	838	63	775
269	65.4	1558	259	1299
269	143	2459	126	2333
269	190	2243	53	2190
269	245	2111	56	2055
269	303	1978	308	1670

4. Conclusions

The present study explores bubble dynamics in two parallel trapezoid microchannels. The following conclusions may be drawn from the results of this study.

1. Similar to that in a single microchannel, the bubbles in two parallel microchannels generally grow linearly with time. For the highest mass flux of this study, the bubble growth rate increases with increase in heal flux, while a reversed trend is demonstrated for the two low mass flow rates due to the movement of the ONB location toward upstream and presence of two-phase flow instability.
2. For the two low mass flow rates of this study, the bubble in slug flow expands very quickly in the axial directions both forward and backward with bubble length increasing exponentially with time due to the evaporation of the thin liquid film between the bubble and heating wall. However, due to the liquid pressure limitation effect, the coefficient of exponent is much smaller than that from the evaporation of thin liquid film around the bubble.
3. Similar to that in the single microchannel, the bubble departure in the two parallel microchannels is also governed by surface tension and drag due to bulk two-phase flow.

Acknowledgments

This work was stimulated by a visiting research of the corresponding author (CP) at the University of Oxford, Oxford, England, UK with Dr. David Kenning in the summer of 1998. This study was supported by the National Science Council of Taiwan, ROC, under the contract of NSC-90-2212-E-007-103.

References

[1] S.G. Kandlikar, M.E. Steinke, S. Tian, L.A. Campbell, High speed photographic observation of flow boiling of water in parallel minichannels, in: Proc. of the ASME National Heat Transfer Conf., 2001.
[2] H.Y. Li, P.C. Lee, F.G. Tseng, C. Pan, Two-phase flow instability of boiling in a double microchannel system at high heating powers, in: Proc. of 1st Int. Conf. in Microchannels and Minichannels, Rochester, NY, USA, 2003.
[3] J.D. Lee, C. Pan, Dynamics of multiple parallel boiling channel systems with forced flows, Nucl. Eng. Des. 192 (1999) 31–44.
[4] D.B.R. Kenning, Private discussion during a summer visiting research of C. Pan at the Oxford University, UK, 1998.

[5] G. Hetsroni, D. Klein, A. Mosyak, S. Segal, E. Pogrbnya, Convective boiling in parallel micro-channels, in: Proc. of 1st Int. Conf. on Microchannels and Minichannels, Rochester, NY, USA, 2003, pp. 59–67.
[6] M.E. Steinke, S.G. Kandliker, Flow boiling and pressure drop in parallel flow microchannels, in: Proc. of 1st Int. Conf. on Microchannel and Minichannels, Rochester, NY, USA, 2003, pp. 567–579.
[7] P.C. Lee, F.G. Tseng, Chin Pan, Bubble dynamics in microchannels, (I) Single microchannel, Int. J. Heat Mass Transfer, in press.